Nanoscale Advances

ROYAL SOCIETY OF CHEMISTRY

PAPER

View Article Online
View Journal | View Issue

Cite this: *Nanoscale Adv.*, 2021, **3**, 5027

A new strategy for improving the electrochemical performance of perovskite cathodes: pre-calcining the perovskite oxide precursor in a nitrogen atmosphere†

Jing Chen,[a] Zhenxiang Zhao,[a] Yu Feng,[a] Xuzhuo Sun,[a] Bo Li,[a] Dongjin Wan[a] and Yuan Tan *[b]

Increasing the concentration of oxygen deficiency in perovskite oxides by suitable cation doping or anion doping can significantly increase the cathode ionic conductivity, thus improving the oxygen reduction reaction activity in solid oxide fuel cells (SOFCs). Herein, pre-calcining the perovskite oxide precursor in N_2 atmosphere is a new strategy to further improve the oxygen non-stoichiometry (δ) and electrocatalytic activity of the cathode. The obtained nitrogen-treated $Sm_{0.5}Sr_{0.5}CoO_{3-\delta}$ (SSC) powder has higher oxygen non-stoichiometry than the untreated one. The δ value is 0.27 for SSC-400 at 800 °C in air. The obtained nitrogen-treated SSC-400 cathodes calcined at 1000 °C show improved electrochemical performance compared to SSC–air, achieving the polarization resistance (R_p) values to be 0.035, 0.078 and 0.214 Ω cm^2 at 700 °C, 650 °C and 600 °C. The maximum power density of the cell with the SSC-600 cathode reaches 0.87, 1.16 and 1.24 W cm^{-2} at 600, 650 and 700 °C, which are more excellent than SSC–air. Pre-calcining the perovskite oxide precursor in N_2 at a suitable temperature can remarkably improve the electrochemical capability of the cathode and provide a convenient and useful strategy to alleviate the problem of oxygen deficiency in perovskite oxides.

Received 12th January 2021
Accepted 28th June 2021

DOI: 10.1039/d1na00031d

rsc.li/nanoscale-advances

1 Introduction

A solid oxide fuel cell (SOFC) is a device that converts chemical energy in hydrocarbon fuels directly into electrical energy and heat energy.[1–3] There are many advantages such as high efficiency, vibration-free operation, silent and fuel flexibility, and insignificant NO_x and SO_x emissions.[4–6] Over the past two decades, nanotechnology and the new cathode materials with high catalytic performance have been used to reduce the operating temperatures.[7–10]

Many scientists have tried reducing the operating temperature of SOFC from 800 to 1000 °C to an intermediate and low temperature (ILT) range of 500–700 °C.[7,11–15] However, the decrease in the working temperature is usually accompanied by a sharp increase in the cathode polarization loss. The activation energy required for oxygen ion transport and the reduction of oxygen molecules to oxygen ions increases dramatically as the operating temperature decreases. Therefore, it is important to improve the oxygen ion conductivity and diffusion ability of the electrode for SOFC at intermediate and low temperatures.

It is convinced that the catalytic capability of perovskite oxides is dramatically related to oxygen deficiency, which changes the surface chemistry, crystal structures and electronic configuration.[9,16] The cobalt-based and ferrite-based ABO_3 perovskite oxides introduce oxygen defects by cation doping at A or B sites.[17–19] The oxygen deficiency in the cobalt or ferrite-based perovskite oxides creates a way of oxide ion transfer. The oxygen deficiency coupled to mixed cobalt valence states[20] makes them suitable for mixed ionic and electronic conductivity (MIEC) electrodes in ILT-SOFC.[21] In recent years, the oxygen anion sites are partially substituted by anion doping for ABO_3 perovskite oxides, such as F^-, H^-, S^{2-}, Cl^-, or N^{3-}. Jin and Co-workers[22] embedded F^- into BSCF and $SrCo_{0.9}Nb_{0.1}O_{3-\delta}$ to improve the oxygen permeability of membranes at intermediate temperatures. It is reported that F^- embedded into cobalt-free $SrFeO_{3-\delta}$ effectively improves the oxygen reduction activity compared to the parent oxide.[23,24]

In this study, a new method to increase the oxygen reduction activity of $Sm_{0.5}Sr_{0.5}CoO_{3-\delta}$ (SSC) by pre-calcining the perovskite oxide precursor in a nitrogen atmosphere was reported, and the precursor was prepared by a traditional citrate sol–gel method. It was found that the N_2-treated process affected SSC in various aspects, such as the morphology, crystal structure, and

[a]School of Chemistry and Chemical Engineering, Henan University of Technology, Zhengzhou 450001, China

[b]The Key Laboratory of Optoelectronic Chemical Materials and Devices, School of Chemical and Environmental Engineering, Jianghan University, Wuhan 430056, China. E-mail: tanyuan@jhun.edu.cn

† Electronic supplementary information (ESI) available. See DOI: 10.1039/d1na00031d

oxygen non-stoichiometry. It is possible to promote the oxidation of Co^{3+} in the nitrogen atmosphere, thereby increasing the oxygen vacancies. The obtained N_2-treated SSC cathodes showed improved electrochemical performance as compared with untreated SSC cathodes. Furthermore, the effect of the nitrogen atmosphere processing on SSC was revealed, which may provide a convenient and useful method to improve the catalytic performance of the perovskite cathode for ILT-SOFCs.

2 Experimental

The SSC powder was prepared by a typical sol–gel method with ethylenediaminetetraacetic acid and citric acid. The analytical grade $Sm(NO_3)_3 \cdot 6H_2O$, $Co(NO_3)_2 \cdot 6H_2O$ and $Sr(NO_3)_2$ were dissolved in deionized water for preparing a solution with a molar ratio of Sm : Sr : Co = 1 : 1 : 2. Then, EDTA and citric acid were dissolved in the solution at a molar ratio of EDTA : total metal ions : citric acid = 1 : 1 : 2, and the pH of the solution was adjusted to approximately 6 by the addition of $NH_3 \cdot H_2O$.[25]

The solution was stirred at 80 °C for 6 h using a magnetic agitator and then dried at 180 °C in an oven to form a black precursor, which was grinded and calcined at 400, 600 and 800 °C in a nitrogen atmosphere for 2 h, respectively. Then, the black powders were reheated in an air atmosphere at 900 °C for 2 h, and the obtained SSC powders were denoted by SSC-400, SSC-600 and SSC-800, respectively. For comparison, the precursor was calcined directly at 900 °C in an air atmosphere for 2 h. The product was denoted as SSC–air.

The crystal microstructure of SSC composite oxides was examined by X-ray diffraction (XRD, Bruker D8 advance, with Cu-Kα radiation, refined slow scan test parameters: 20–80°, scanning speed: 10° min^{-1}) analysis. The valence state of Co and O in SSC samples was studied by X-ray photoelectron spectroscopy (XPS, Escalab 250XI). The XPS spectrogram was analyzed using the XPSPEAK software. The numerical values of binding energy (B.E.) were corrected with carbon (C 1s = 284.5 eV) as the internal standard.

First, the oxygen vacancies of the SSC samples were measured by iodometric titration,[26,27] and then the oxygen vacancies were obtained using thermogravimetric (TG) analyzer. TG (METTLER TOLEDO-TGA/DSC 2) was used to measure the weight loss of powder at a heating rate of 10 °C min^{-1} from 25 °C to 800 °C. Non-stoichiometry oxygen concentrations at different temperatures were calculated based on TG data. The non-stoichiometry oxygen was calculated using the following formula:

$$\delta = \frac{M \times m_0 - (M - 15.9994 \times \delta_0) \times m}{15.9994 \times m_0}$$

M is the molar mass of SSC, δ_0 is the non-stoichiometry oxygen of the sample at room temperature (the data is shown in Table S2†), m_0 is the initial weight, and m is the actual weight after the sample was heated, and M is the molar mass of the stoichiometric form of $Sm_{0.5}Sr_{0.5}CoO_3$ (M_{SSC} = 225.92).

The electrochemical capability of the sample was measured using an SDC-based symmetric cell. A dense SDC pellet of 13 mm diameter was produced by die casting using SDC ($Sm_{0.1}Ce_{0.9}O_{2-\delta}$, Fuel Cell Materials, USA) powders, and then sintered in air at 1450 °C for 5 h. Electrode slurry was prepared by mixing the SSC powder and binder in an agate mortar. The slurry was screen-printed on both sides of the SDC pellets to form symmetric cells, and the cells were calcined at temperatures of 950, 1000 and 1050 °C, respectively. The cathode layer was coated with platinum as a collecting layer and sintered at 800 °C for 1 h. The electrochemical impedance spectroscopy (EIS) of the cells was tested in air from 550 °C to 750 °C, which use an electrochemical workstation (Zennium) at 0.01 Hz to 1 MHz. The morphologies of the SSC powders and the symmetric cells were tested by scanning electron microscopy (SEM) using a HT7700 Exalens microscope.

Anode-supported single cells were fabricated for electrochemical performance evaluation with the structure of NiO-GDC|GDC|SSC. The anode substrates were produced by die casting with 13 mm diameter using a mixture of NiO (Sigma-Aldrich, USA) and GDC ($Gd_{0.1}Ce_{0.9}O_{2-\delta}$, Fuel Cell Materials, USA) powders with a NiO : GDC weight ratio of 60 : 40, and carbon black was used as a pore former. The anode was sintered at 1100 °C for 2 h.[9] The GDC electrolyte slurry was printed on the pre-calcined NiO-GDC anode, and the anode/electrolyte was sintered at 1500 °C for 5 h to obtain a dense electrolyte. The SSC slurry was screen printed on the GDC electrolyte and sintered at 1050 °C for 2 h at a heating rate of 5 °C min^{-1} to obtain the SSC cathode.

3 Results and discussion

3.1 Property of SSC powders

In order to study the influence of calcination atmosphere and temperature on the crystal structure, first, the precursor of the sample undergoes thermal sintering in the nitrogen atmosphere and then undergoes calcination in the air atmosphere. Fig. 1a shows the XRD pattern of the SSC powders annealed under different heat-treatment conditions. After the SSC powder was heated at 900 °C for 2 h in air, the SSC–air powder exhibits the obvious splitting of a tetragonal perovskite phase (*I*4/*mmm* space group) at 32.9–33.6° in Fig. 1b. As the calcination temperature increases, the XRD pattern shows that the peak at about 33° gradually merges from two peaks into a single peak, and SSC-800 still shows the tetragonal phase (*I*4/*mmm* space group), as shown in Fig. 1c. No impurity phase was observed in the XRD pattern below 800 °C in the N_2 atmosphere. The impurity phase emerges when the SSC powder in N_2/Ar was heated to temperatures above 1000 °C. Table S1† presents the crystallographic parameters of SSC, which were calculated from the XRD image. After the nitrogen atmosphere treatment, the cell volume increases gradually with the increase in temperature. However, the cell volume of the SSC–air sample is close to that of the samples treated with nitrogen at 600 °C.

Fig. 2 shows the SEM images of different SSC powders. Fig. 2a shows SSC-400 calcined at 400 °C in a N_2 atmosphere. It could be discovered that the powder particles are loose and dispersed well, and there is no significant aggregation in the sample. As the temperature increases, the accumulation of SSC particles is more and more serious, as shown in Fig. 2c. The

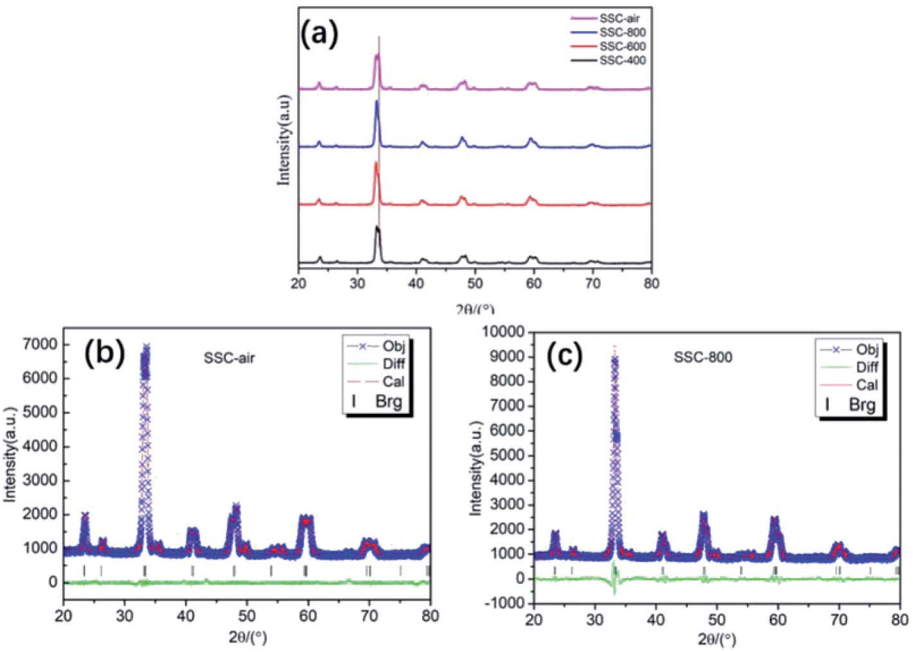

Fig. 1 (a) XRD image of the $Sm_{0.5}Sr_{0.5}CoO_{3-\delta}$ powders under different conditions: SSC–air is the precursor without treatment; SSC-800 is the precursor sintered at 800 °C for 2 h in N_2; SSC-600 is the precursor sintered at 600 °C for 2 h in N_2; SSC-400 is the precursor sintered at 400 °C for 2 h in N_2. Rietveld refinement profiles of (b) SSC–air and (c) SSC-800 to powder XRD collected at room temperature.

SSC–air powder without N_2 treatment reveals a broader grain size distribution, from sub-micrometric grains to nearly 5 μm diameter grains, as shown in Fig. 2d. After the treatment of the SSC precursor in N_2 below 600 °C, the aggregation of the nanoparticles can be impressed significantly. It seems possible that the SSC-400 and SSC-600 powders have high surface area, which causes the increase in calcination activity of the powders. Fig. S1† shows the microstructural images of the SSC at high magnification. The size of the SSC particles treated with N_2 gradually decreases and the agglomeration is more serious as the sintering temperature increases. The untreated SSC powder has a broad distribution of particle size.

In order to understand the effect of temperature and atmosphere on the properties of SSC, the process of

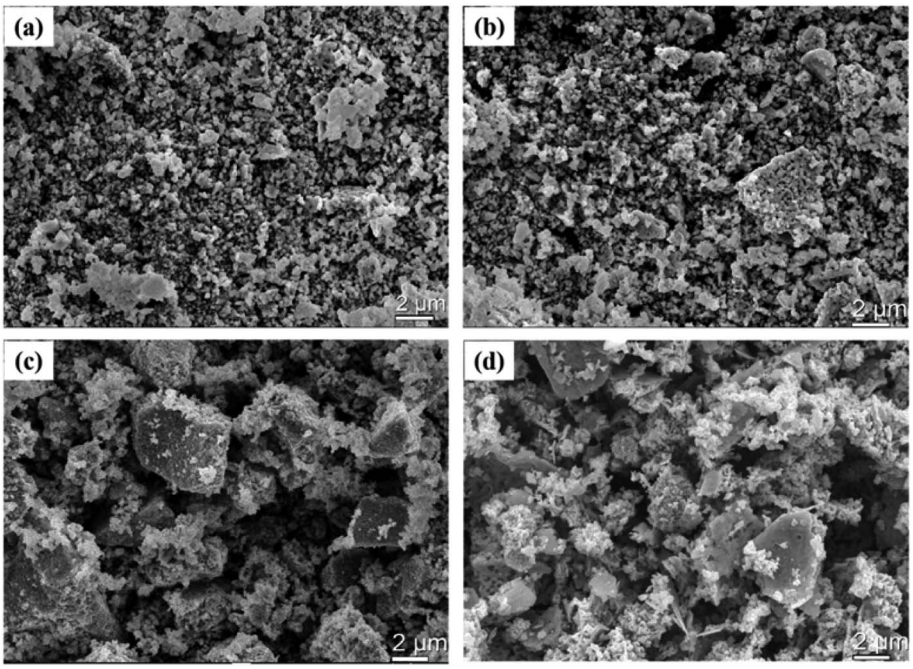

Fig. 2 SEM images of SSC powders: (a) SSC-400; (b) SSC-600; (c) SSC-800; and (d) SSC–air, untreated.

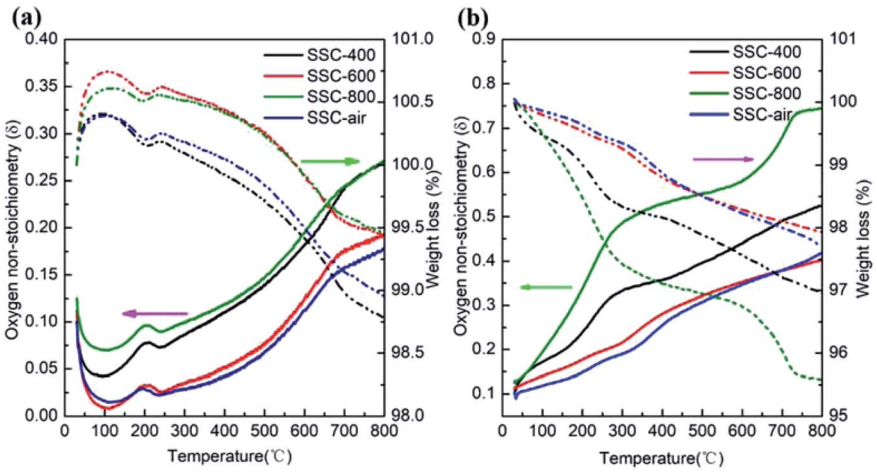

Fig. 3 Oxygen non-stoichiometry and TG plots of the SSC annealed under different conditions. TG was measured in (a) air atmosphere and (b) N_2 atmosphere.

nonstoichiometric oxygen evolution was studied. The oxygen non-stoichiometry (δ) of SSC powders was obtained by iodometric titration combined with TG data.[9] As shown in Table S2,† the values of δ at room temperature are 0.10, 0.10, 0.11 and 0.13 for SSC–air, SSC-400, SSC-600 and SSC-800, respectively. Fig. 3 shows the experimental results of δ and thermogravimetry of SSC tested in the air and N_2 atmosphere. Fig. S3(b)† shows the experimental results of δ and thermogravimetry of SSC, which pre-calcined at 600 °C at different concentrations of hydrogen (0%, 5%, 10% H_2/N_2). The δ increases with the increase in measured temperatures at all atmospheres. In particular, the δ value of SSC-400 and SSC-800 increased significantly with the increase in temperature. The δ values are 0.27 and 0.27 in air (Fig. 3a), and 0.53 and 0.74 in N_2 (Fig. 3b) for SSC-400 and SSC-800 at 800 °C, respectively. The oxygen vacancy of the samples pre-calcined in the nitrogen atmosphere of the SSC precursor was higher than that of the untreated sample, indicating that the pre-calcination of the precursor in N_2 at an appropriate temperature can increase the oxygen vacancies of the sample. Samples treated in the nitrogen atmosphere are very sensitive to oxygen partial pressure, and oxygen vacancies increase rapidly with temperatures in the N_2 atmosphere. For example, δ of SSC-800 is as high as 0.74 at 800 °C. The δ value of BSCF as measured by Kriegel *et al. via* isothermal thermogravimetry at 850 °C is 0.69(ref. 28) and δ was derived from neutron diffraction data, as reported by Mcintosh *et al.*[29] SSC powders pre-calcined in the nitrogen atmosphere possessing high δ may have two main factors: (1) the precursors prepared by EDTA and citric acid as templates and the fuel were pre-treated under a flow of N_2, which facilitates the introduction of C atoms in the sample. After subsequent calcination, C combined with O_2 to form CO_2. During the combustion process, the local partial pressure of oxygen is lower, which is favorable for forming defects. (2) The reducing atmosphere could inhibit the oxidation of Co^{3+} to Co^{4+}, thereby facilitating the formation of oxygen vacancies.[30]

The chemical states of Co and O in SSC samples were studied by XPS (C 1s peak at 284.5 eV). The oxidation states are identified and quantified by the peaks of Co $2p_{3/2}$, Co $2p_{1/2}$ and O 1s. In general, in $SmCoO_3$, when Sm^{3+} is partially replaced by the bivalent element Sr, the Co ion presents a mixed valence state. As shown in Fig. 4a, Co 2p has four obvious peaks. The corresponding binding energies of these four peaks are 780.09, 782.4, 795.4 and 797.1 eV, respectively. The weak peaks at 785.8, 801.5, 790.2 and 805.6 eV correspond to satellite peaks. The

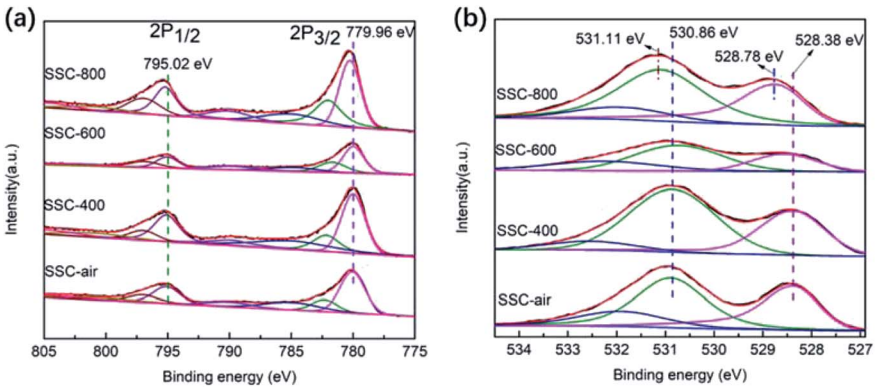

Fig. 4 (a) XPS image of Co 2p and (b) XPS image of O 1s for the SSC–air, SSC-400, SSC-600 and SSC-800 powders.

peaks at the two weak shake-up satellites with the combined energy of 782.4, 797.1 eV and 785.8, 801.5 eV can be identified as Co^{4+}, and the peaks of other shake-up satellites appearing at 780.09, 795.4 eV and 790.2, 805.6 eV could be attributed to Co^{3+}. The result was inconsistent with the literature.[18,19] In Fig. 4b, the O 1s image has two obvious peaks, and the corresponding binding energies of two peaks are 528.4 eV and 530.9 eV respectively. The peaks at 528.4 eV can be identified as lattice oxygen, and the peaks at 530.9 eV belong to adsorbed oxygen.[20,21]

In this study, iodine titration was used to observe the change in the non-stoichiometric oxygen of SSC. At room temperature, the non-stoichiometric oxygen of SSC treated with nitrogen increased gradually, as the ratio of Co^{4+}/Co^{3+} increased with the increase in treatment temperature (the specific data are shown in Table S3†). In addition, the concentration of oxygen vacancy increased according to eqn (1), which is consistent with the study of Mefford.[22] At the same time, through the analysis of the XPS spectrum of O 1s (the specific data are shown in Table S4†), the proportion of adsorbed oxygen increases, indicating that nitrogen treatment does has a positive effect on the concentration of SSC oxygen vacancy.

$$SmCoO_3 + xSr^{2+} - xSm^{3+} \rightarrow Sm_{1-x}Sr_xCo_y^{3+}Co_{1-y}^{4+}O_{3-\delta} + \frac{\delta}{2}O_2 \quad (1)$$

3.2 Morphology of SSC cathodes

The microstructure images of the different cathodes are shown in Fig. 5 and S2.† From the images, the difference is obvious between cathodes prepared at different pre-calcination temperatures in the N_2 atmosphere. As the pre-sintering temperature increases, the SSC grain size gradually grows. The fracture area of the SSC-800 cathode (Fig. 5c) is larger than that of the SSC-600 cathode (Fig. 5b). The SSC-800 cathode showed severe grain sintering (Fig. 5c), and the surface SEM images of the SSC-800 cathode exhibited a grain diameter of approximately 1 μm (Fig. S2†). In contrast to the SSC–air cathode, the SSC powders pre-calcined in N_2 have higher sintering properties. We confirm that there are two factors that promote electrode sintering: (1) high oxygen vacancies help to promote the sintering of the sample. As shown in Fig. 3, the sample treated with nitrogen has more oxygen vacancies. SSC-800 has the highest oxygen vacancies under testing temperatures in both air and nitrogen, and therefore, the sample had the most aggressive sintering. (2) The powder is composed of particles with different sizes, which is advantageous for promoting the sintering of the sample. As shown in Fig. 2, SSC-800 has a wide range of particle size distribution, which is helpful for sintering. Fig. 6 shows the cross-sectional images of the SSC-400 and SSC-800 cathodes calcined at 950 and 1000 °C. It could be found that as the calcination temperature decreases, the electrode particles are gradually decreased, and sintering of the electrode particles is also significantly reduced.

3.3 Electrochemical performance analysis

The electrochemical capability of SSC cathodes was tested by EIS. The performance of the electrode was dramatically related to the sintering temperature of the electrodes, and most cathodes were sintered at temperatures above 1000 °C.[31] As shown in Fig. 5 and 6, the morphology of the cathodes changed significantly with different temperatures. In this study, the EIS was tested for SSC-400, SSC-600, SSC-800 and SSC–air cathodes sintered at 1050 °C, 1000 °C and 950 °C. The ohmic resistance was subtracted, and the polarization resistance (R_p) was calculated using the Nyquist plot. Fig. 7 shows the R_p value of the cathodes calcined at different temperatures. At a calcining temperature of 1050 °C, the SSC-800 cathode has higher R_p than other cathodes, and the values of R_p are 0.21 and 0.47 Ω cm^2 at

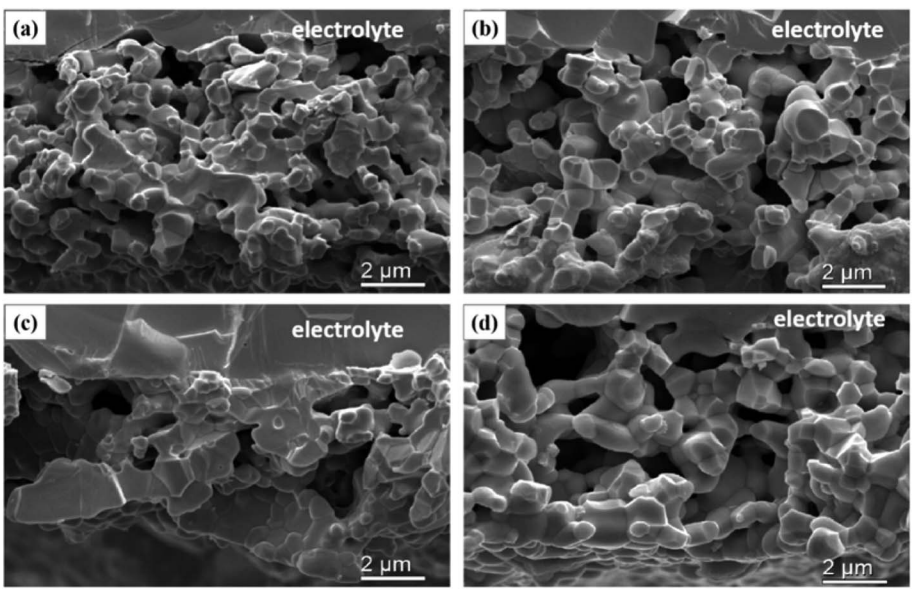

Fig. 5 SEM images of SSC cathodes (cross section) sintered at 1050 °C: (a) SSC-400; (b) SSC-600; (c) SSC-800; and (d) SSC–air.

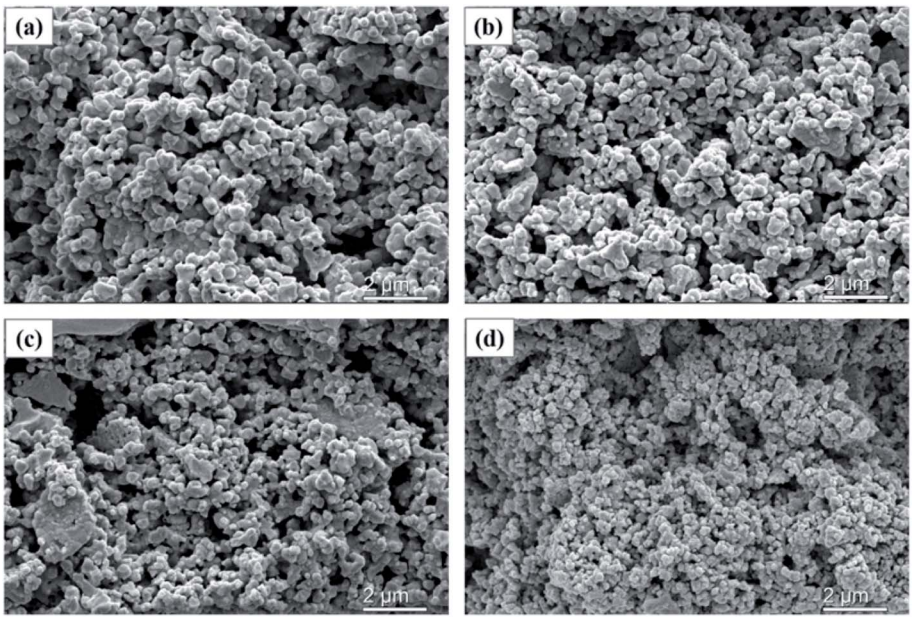

Fig. 6 SEM images of SSC cathodes (cross section) sintered at 1000 and 950 °C: (a) SSC-400 (1000 °C); (b) SSC-400 (950 °C); (c) SSC-800 (1000 °C); and (d) SSC-800 (950 °C).

700 and 650 °C. For the SSC-600 cathode, the R_p values are 0.07 and 0.15 Ω cm^2 at 700 and 650 °C. The active energy for SSC-800 cathode is 97.82 kJ mol^{-1} (1.01 eV) and 105.18 kJ mol^{-1} (1.09 eV) for the SSC-600 cathode, respectively (Table 1). The activation energy was the smallest for the cathodes calcined at 1050 °C, and this may be related to the severe sintering of the electrode.

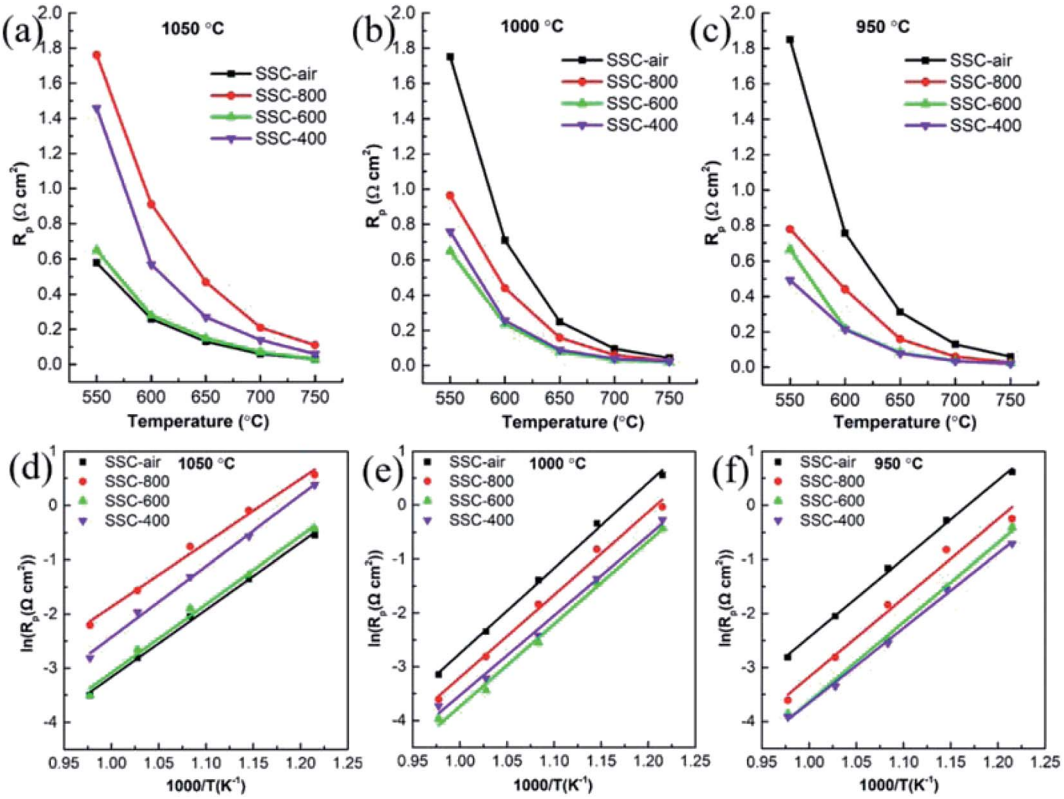

Fig. 7 R_p values of the cathodes heated at (a) 1050 °C, (b) 1000 °C and (c) 950 °C at different temperatures. Arrhenius plots for the cathodes calcined at (d) 1050 °C, (e) 1000 °C and (f) 950 °C.

Table 1 Active energy of cathodes calcined at 1050, 1000 and 950 °C

	Active energy, kJ mol^{-1}		
Sample	1050 °C	1000 °C	950 °C
SSC–air	103.31	131.67	120.65
SSC-800	97.82	127.68	121.39
SSC-600	105.18	127.53	122.27
SSC-400	108.99	123.46	115.42

The activation energy for cathodes sintered at a temperature of 1000 °C is bigger than that at 950 °C, which can possibly be attributed to the larger average grain sizes at 1000 °C.

The higher oxygen vacancy of the SSC-800 powder (Fig. 2) is beneficial for the grain contact, and the grain size is bigger than those obtained by other powders, as shown in Fig. 5. The big grain size and good contact facilitate electronic and ionic conduction between the particles.[9] However, the cathode with large particles has a small surface area and porosity, which is disadvantageous to the diffusion and adsorption of oxygen onto the electrode surface. The SSC-400 powder has approximate oxygen vacancy with SSC-800, and there is also severe sintering between the particles for SSC-400, as shown in Fig. 5a. The cathode of SSC-400 shows the poor electrochemical performance for ORRs. The catalytic performance and the morphology of the cathodes change with the calcining temperature. The SSC electrodes treated with N_2 have lower values of R_p than the untreated electrode SSC–air, as shown in Fig. 7b and c at 1000 and 950 °C, respectively. For SSC-400 cathode calcined at 950 °C, the R_p values are 0.214, 0.078 and 0.035 Ω cm^2 at 600, 650 and 700 °C, respectively. The value is lower than that of the nano-structured SSC-FD cathode.[32] The active energy for the SSC-400 cathode is 115.42 kJ mol^{-1} (1.20 eV).

The particles size of SSC-400 is bigger than that of SSC-800 calcined at 950 °C, as shown in Fig. 6, which may be related to the initial particle size of the powders (as shown in Fig. 2). The smaller the particles that make up the cathode, the less conducive they are to the bulk diffusion process of oxygen ions. Therefore, the electrochemical performance of SSC-800 is inferior to that of SSC-400.

The high electrochemical performance of the SSC-400 cathode for ORRs is mainly related to the following factors: (1) the high oxygen vacancy concentration of the cathode enhances the bulk and surface exchange properties for ORRs;[33,34] (2) the good connectivity between the electrode particles facilitates the conduction of ions and electrons; and (3) the large surface area facilitates the diffusion and adsorption of oxygen.

Fig. 8 shows the current–voltage relationship of single cells with different SSC cathodes at different operating temperatures. The maximum power densities (P_{max}) of the single cell with the SSC-400 cathode reach 0.84, 0.84 and 0.80 W cm^{-2} at 650, 700 and 750 °C. The values of P_{max} are 0.82 W cm^{-2}, 0.82 W cm^{-2} and 0.63 W cm^{-2} at 650, 700 and 750 °C for cells with the SSC-800 cathode. It is very interesting to observe that the P_{max} value at 650 °C is almost the same as that at 700 °C for both the single cell with the SSC-400 cathode and SSC-800 cathode, while the single cell with SSC-600 cathode, presented a greatly enhanced performance. As shown in Fig. 8b, the P_{max} value at 650 °C is as

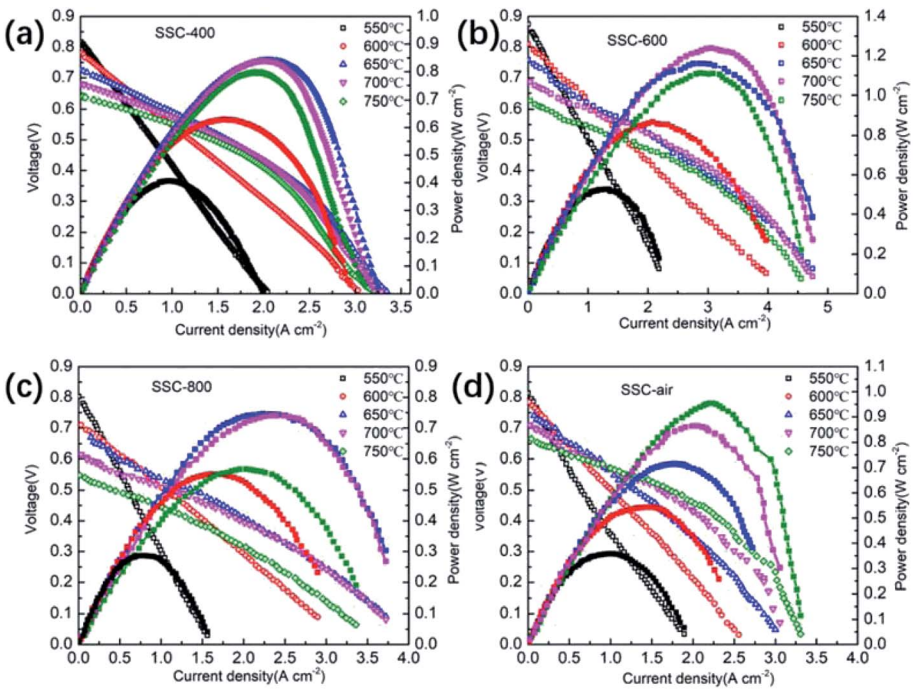

Fig. 8 Current voltage curves of single cells with cathodes sintered at 1050 °C: (a) SSC-400, (b) SSC-600, (c) SSC-800, and (d) SSC–air, and the cells were tested with hydrogen and air at different temperatures.

high as 1.16 W cm^{-2}, which is almost equal to the value of 1.24 at 700 °C. It can be found that the samples with the cathode pre-calcined in the N_2 atmosphere had a higher P_{max} at 650 °C than the value at 750 °C. Moreover, the sample of SSC–air without N_2 pre-treatment for the cathode had the highest P_{max} value at 750 °C. Among these four samples, P_{max} of SSC-600 was higher than that of SSC–air, showing excellent electrochemical performance. This result is also in accord with the results of the symmetry cells shown in Fig. 7a. The experimental results show that the pre-calcination of the precursor powder under N_2 flow is beneficial to optimize the electrode structure (as shown in Fig. 5) and ultimately affect the electrochemical performance of cells.

The sol–gel method is a commonly used chemical method for preparing cathode powder. It was found that pre-sintering the precursor at different temperatures in the nitrogen atmosphere will ultimately affect the electrochemical performance of the electrode. The R_p value of the symmetrical cells treated in nitrogen was significantly lower than that of the samples calcined directly in air in the range of 650–750 °C. The results of the single cells further confirmed that the powder treated in the nitrogen atmosphere has excellent catalytic performance from 650 to 700 °C, and the maximum power density of cells at 650 and 700 °C is higher than the peak power density at 750 °C. The nitrogen atmosphere treatment of the precursor will eventually improve the catalytic performance of the electrode at 650–700 °C. The main reasons are as follows: (1) with the increase in sintering temperature, the organic compounds in the precursor would be carbonized and the metal nitrate began to decompose. When the carbonized sample is calcined again in air, the carbon in the sample will react with oxygen to produce CO_2, which may be accompanied by the decrease in local oxygen partial pressure, resulting in the generation of oxygen vacancies. The oxygen vacancies of SSC are increased and the agglomeration of SSC powder is changed after the precursor is treated in the nitrogen atmosphere, which is beneficial to the sintering of cathodes. (2) At the same calcination temperature for electrodes, the degree of sintering between SSC particles pretreated with nitrogen was higher than that of samples without nitrogen treatment. Therefore, there is a better connection between the electrode particles, which is beneficial to the bulk conduction of oxygen ions. Therefore, the cathode treated with the nitrogen atmosphere exhibits excellent oxygen reduction reaction in the range of 650–700 °C.

4 Conclusion

In summary, the $Sm_{0.5}Sr_{0.5}CoO_{3-\delta}$ powders with high oxygen vacancies can be obtained by pre-calcining the SSC precursor in the nitrogen atmosphere. The nitrogen-treated powders have a high sintering activity, which not only helps to lower the sintering temperature of the electrode, but also avoids chemical reaction between the electrolyte and the electrode due to high preparing temperatures. This result further proves that the pretreatment of the precursor in N_2 at a suitable temperature can greatly improve the catalytic capability of the electrode. For the cathodes calcined at 1000 °C and 950 °C, the nitrogen pretreated samples show improved oxygen reduction activity at intermediate temperatures compared with untreated samples. These results indicate that pre-calcining the SSC precursor in the nitrogen atmosphere provides a convenient and useful strategy for preparing an oxygen-deficient perovskite oxide as a cathode for IT-SOFCs.

Conflicts of interest

There are no conflicts to declare.

Acknowledgements

This work was financially supported by the National Key Research & Development Program of China (2018YFE0124700), National Natural Science Foundation of China (51872103), Natural Science Foundation of Henan (212300410035, 182102210398), and State Key Laboratory of Materials Processing and Die & Mould Technology, Huazhong University of Science and Technology (P2019-004).

References

1 K. Al-Khori, Y. Bicer and M. Koc, *J. Cleaner Prod.*, 2020, **245**, 18.
2 N. Sazali, W. N. W. Salleh, A. S. Jamaludin and M. N. M. Razali, *Membranes*, 2020, **10**, 18.
3 S. Longo, M. Cellura, F. Guarino, G. Brunaccini and M. Ferraro, *Sci. Total Environ.*, 2019, **685**, 59–73.
4 W. Zhou, Y. Jiao, S.-D. Li and Z. Shao, *ChemElectroChem*, 2016, **3**, 193–203.
5 T. M. Gür, *Prog. Energy Combust. Sci.*, 2016, **54**, 1–64.
6 N. Mahato, A. Banerjee, A. Gupta, S. Omar and K. Balani, *Prog. Mater. Sci.*, 2015, **72**, 141–337.
7 M. Li, M. Zhao, F. Li, W. Zhou, V. K. Peterson, X. Xu, Z. Shao, I. Gentle and Z. Zhu, *Nat. Commun.*, 2017, **8**, 13990.
8 Y. Zhu, W. Zhou, Y. Chen and Z. Shao, *Angew. Chem., Int. Ed.*, 2016, **55**, 8988–8993.
9 J. Chen, X. Yang, D. Wan, B. Li, L. Lei, T. Tian, B. Chi and F. Chen, *Electrochim. Acta*, 2020, **341**, 136031.
10 J. F. Shin, W. Xu, M. Zanella, K. Dawson, S. N. Savvin, J. B. Claridge and M. J. Rosseinsky, *Nat. Energy*, 2017, **2**, 16214.
11 Z. Gao, L. V. Mogni, E. C. Miller, J. G. Railsback and S. A. Barnett, *Energy Environ. Sci.*, 2016, **9**, 1602–1644.
12 Y. Chen, B. deGlee, Y. Tang, Z. Wang, B. Zhao, Y. Wei, L. Zhang, S. Yoo, K. Pei, J. H. Kim, Y. Ding, P. Hu, F. F. Tao and M. Liu, *Nat. Energy*, 2018, **3**, 1042–1050.
13 F. S. da Silva and T. M. de Souza, *Int. J. Hydrogen Energy*, 2017, **42**, 26020–26036.
14 D. Sari, F. Piskin, Z. C. Torunoglu, B. Yasar, Y. E. Kalay and T. Ozturk, *Solid State Ionics*, 2018, **326**, 124–130.
15 B. An, W. Zhou, Y. Guo, R. Ran and Z. Shao, *Int. J. Hydrogen Energy*, 2010, **35**, 5601–5610.
16 Q. Ji, L. Bi, J. Zhang, H. Cao and X. S. Zhao, *Energy Environ. Sci.*, 2020, **13**, 1408–1428.

17 W. Fan, Z. Sun, Y. Bai, K. Wu, J. Zhou and Y. Cheng, *J. Power Sources*, 2020, **456**, 228000.
18 J. Zhang, X. Li, Z. Zhang, X. Xu, Y. Chen, Y. Song, J. Dai, G. Yang, R. Ran, W. Zhou and Z. Shao, *J. Power Sources*, 2020, **457**, 227995.
19 S. P. Jiang, *Int. J. Hydrogen Energy*, 2019, **44**, 7448–7493.
20 A. K. Eriksson, S. G. Eriksson, L. C. Chapon and C. S. Knee, *Mater. Res. Bull.*, 2010, **45**, 1875–1882.
21 M. A. Javed, M. Muneer, G. Abbas, I. Shakir, R. Batool, M. Iqbal, M. Hussain, Z. U. Rehman and R. Raza, *Ceram. Int.*, 2020, **46**, 10348–10355.
22 J. Zhu, G. Liu, Z. Liu, Z. Chu, W. Jin and N. Xu, *Adv. Mater.*, 2016, **28**, 3511–3515.
23 H. X. Dai, C. F. Ng and C. T. Au, *J. Catal.*, 2000, **189**, 52–62.
24 E. J. Moon, Y. J. Xie, E. D. Laird, D. J. Keavney, C. Y. Li and S. J. May, *J. Am. Chem. Soc.*, 2014, **136**, 2224–2227.
25 Y. M. Guo, H. G. Shi, R. Ran and Z. P. Shao, *Int. J. Hydrogen Energy*, 2009, **34**, 9496–9504.
26 X. N. Jiang, J. Wang, G. Q. Jia, Z. J. Qie, Y. C. Shi, A. Idrees, Q. Y. Zhang and L. Jiang, *Int. J. Hydrogen Energy*, 2017, **42**, 6281–6289.
27 J. L. Sun, X. M. Liu, F. Han, L. L. Zhu, H. L. Bi, H. P. Wang, S. L. Yu and L. Pei, *Solid State Ionics*, 2016, **288**, 54–60.
28 R. Kriegel, R. Kircheisen and J. Töpfer, *Solid State Ionics*, 2010, **181**, 64–70.
29 S. Mcintosh, J. F. Vente, W. G. Haije, D. H. A. Blank and H. J. M. Bouwmeester, *Solid State Ionics*, 2006, **177**, 1737–1742.
30 Y. Lu, L. Chen, C. Lu, Y. Ni and Z. Xu, *J. Rare Earths*, 2013, **31**, 1183–1190.
31 C. Su, X. Xu, Y. Chen, Y. Liu, M. O. Tadé and Z. Shao, *J. Power Sources*, 2015, **274**, 1024–1033.
32 L. M. Acuna, J. Pena-Martinez, D. Marrero-Lopez, R. O. Fuentes, P. Nunez and D. G. Lamas, *J. Power Sources*, 2011, **196**, 9276–9283.
33 C. Sun, Y. Kong, L. Shao, K. Sun and N. Zhang, *J. Power Sources*, 2020, **459**, 228017.
34 C. Sowjanya, R. Mandal, S. Abhinay, A. Mohanta, S. Das and S. K. Pratihar, *J. Solid State Chem.*, 2020, **285**, 121237.